ZOOLOGICAL RESEARCH

Preliminary study on fine structures of subcortical nuclei in rhesus monkeys by *ex vivo* 9.4 T MRI

DEAR EDITOR,

Changes in fine structures of the brain over a life span can have robust effects on neural activity and brain function, which both play crucial roles in neurodegenerative diseases. Clinically, however, low-resolution MRI only provides limited information about fine brain structures. Here, using high-resolution 9.4 T MRI, we established a set of structural images and explored the fine structures of the claustrum, hippocampus, amygdala complex, and subregions of the amygdala complex (BLA, including lateral, basal, and accessory basal subnuclei) in rhesus macaque (*Macaca mulatta*) brains. Based on these high-resolution images, we were able to discriminate the subregional boundaries accurately and, at the same time, obtain the volume of each brain nuclei. Thus, advanced high-resolution 9.4 T MRI not only provides a new strategy for early diagnosis of neurodegenerative diseases, but also provides the ability to observe fine structural changes in the brain across a life span.

The basolateral complex of the amygdala (BLA), including the lateral, basal, and accessory basal subnuclei, is an important region receiving information from the cortex and subcortical nuclei, including the hippocampus, and transferring information to other parts of the amygdala (Huang et al., 2013; Pikkarainen et al., 1999; Sah et al., 2003; Saunders et al., 1988). Neuroimaging studies have significantly expanded our knowledge of brain structure and function during postnatal development and aging, as well as the progression of neurological and psychological disorders (Knickmeyer et al., 2010; Shaw et al., 2008; Sowell et al., 2002a, 2002b). The introduction of 9.4 T MRI technology has greatly facilitated subcortical classification of brain regions with fine dimensions (Kwan et al., 2017). With its high resolution, we can accurately discriminate subregional boundaries and obtain the volume of each brain nucleus. As an advanced imaging device, 9.4 T MRI provides a new strategy for the early diagnosis of neurodegenerative diseases and can further clarify fine structural changes in the central nervous system over a life span.

Three female rhesus monkeys aged from 12 to 20 years old were used in this study. Postmortem brains of the monkeys were provided by the Kunming Primate Research Center (KPRC) of the Chinese Academy of Sciences (CAS). Details on age and brain volume are provided in Table 1. The brains were acquired following approved protocols from the Kunming Institute of Zoology (KIZ), CAS. Briefly, the monkeys were deeply anesthetized with an overdose of sodium pentobarbital (50 mg/kg i.m.) and perfused transcardially with 0.9% saline followed by 10% buffered formalin. The brains were removed from the skulls and submerged in a 500 mL solution of 4% paraformaldehyde (PFA). Each brain was positioned in an oval-shaped container filled with FOMBLIN® perfluoropolyether (Solvay Specialty Polymers, Italy). The container was generated by 3D printing and was adapted to the outer surface of the brain so that the brain tissue was held steady during scanning. Brains immersed in perfluoropolyether were vacuumed for at least 3 d under 0.1 atmospheric pressure to remove all air bubbles in the sample before the MRI scans. One half of each brain was selected and cut into 50 μm sections through the amygdala along the horizontal plane. Sections were stained with Cresyl violet. All animal care and experimental procedures were carried out in strict accordance with the guidelines for the National Care and Use of Animals approved by the National Animal Research Authority (China) and the Institutional Animal Care and Use Committee (IACUC) of KIZ, CAS, and were approved by the Ethics Committee of KIZ and KPRC, KIZ, CAS (AAALAC

Received: 05 September 2019; Accepted: 30 December 2019; Online: 06 January 2020

Foundation items: This work was supported by the Chinese Academy of Sciences (Y406541141 and 1100050210), National Natural Science Foundation of China (91649119), and Ministry of Science and Technology of China (2015CB755605 and 2016YFC1305902) to J.L.L., National Natural Science Foundation of China (91649101), National Key Research and Development Program of China (2016 YFC1300500-503), Hefei Science Center (2017HSC-KPRD003), and Hefei Institutes of Physical Science (YZJJ201702) to K.Z.

DOI: 10.24272/j.issn.2095-8137.2020.013

Table 1 Specimen information

Specimen ID	Age (Years)	Brain volume (mL)	Cerebellum volume (cm^3)	Hippocampus		Amygdala		Lateral nucleus (L)		Basal nucleus (B)		Accessory basal nucleus (AB)		Claustrum	
				Left	Right	Left	Right	Left	Right	Left	Right	Left	Right	Left	Right
05076	12	73	8.02	482.868	477.4	192.81	196.56	54.34	61.74	36.71	42.48	59.2	60.68	170.345	176.97
00006	18	93	8.57	528.901	539.1	193.62	204.06	50.46	58.59	46.22	44.61	61.72	60.67	200.424	182.19
98374	20.3	93	8.22	528.901	560.6	253.79	262.58	63.51	70.98	38.82	38.45	66.24	67.37	172.501	186.77

accredited).

MRI was performed on a 9.4 Tesla 40 cm MRI system (a superconducting magnet of 9.4 T/400 PS, Agilent Inc., USA, equipped with Avance HD BioSpec console, Bruker BioSpin MRI GmbH, Germany) with a patented transceiver coil. To acquire high-quality MRI images, a newly patented conformal radiofrequency (RF) coil (Chinese Patent application 201710191106.8) based on the standard quadrature RF excitation/receive configuration was used. To achieve high sensitivity, the coil was designed with half open brain-conformal surface mode and composed of 16 distributed resonant elements with quadrature ports. Therefore, only one ^1H channel was used but with sufficient sensitivity for high-resolution imaging. The maximal inner diameter of the coil was 95 mm, which is appropriate to hold the container and produce RF-illuminating volume for the entire brain.

For each macaque brain, T_2* weighted images of FLASH (Fast Low Angle Shot) 2D and 3D sequences were acquired. The 2D images were acquired with the following settings: TR/TE=2 900 ms/14 ms, flip angle=80°, resolution=208 μm×182 μm, slice thickness=0.5 mm, matrix size=384×384, 104 slices, acquisition time=18 m 30 s, band kHz. The FLASH 2D images were acquired eight times separately and averaged to achieve high-resolution images with a better signal-to-noise ratio (SNR). For the 3D images, the following settings were applied: TR/TE=45 ms/13 ms, flip angle=10°, voxel size=155 μm×155 μm×155 μm, matrix size=515×420×354, acquisition time=1 h 51 m 30 s, band kHz.

Currently, there is no precedent for subfield segmentation of the amygdala. In addition, standard analysis software cannot perform automatic segmentation of the amygdala subfields at the above resolution. Manual segmentation of 9.4 T images can be achieved with reference to an atlas (Saleem & Logothetis, 2012) using the ITK-SNAP package. Here, MRI segmentation of the hippocampus, amygdala, basolateral complex in the amygdala (BLA, including the lateral, basal, and accessory basal nuclei), and claustrum were manually performed with reference to the atlas "A Combined MRI and Histology Atlas of the Rhesus Monkey Brain in Stereotaxic Coordinates" (Saleem & Logothetis, 2012). The atlas, which also contains histological sections and images, clearly shows the boundaries of each nucleus for segmentation. The segmented regions were only regions of interest (ROI) and did not exactly match specific histological nuclei. The subregions of interest in the amygdala (sROI) were close to the BLA (ROIs of lateral nucleus, basal nucleus, and accessory basal nucleus, briefly denoted as L, B, AB, and claustrum).

To segment the fine structures on MRI images correctly, both MRI resolution and contrast are crucial parameters. Compared to histological sections before (Figure 1B, middle panel) and after staining (Figure 1B, right panel), the shapes of the subfields in the amygdala on MRIs closely matched those of the subfields in the corresponding histological staining section. This finding laid the foundation for our segmentation of MRI images. After 9.4 T MRI segmentation, we obtained a more accurate nucleus volume than that achieved using 3 T MRI, which was limited by voxel-like reconstruction (voxel size=310 μm×310 μm×300 μm) (Figure 1A). Image intensity was corrected to remove bias before quantitative image segmentation. Image contrast between the amygdala, hippocampus, and claustrum (Figure 1A) was sufficient to identify the landmarks of their structures; however, it was difficult to distinguish the boundaries of each subfield in the BLA and claustrum from the 3 T MRI images (uMR 790 United Imaging Inc., China). The 3D T2 sequences at 3 T were acquired with the following settings: TR=2 500 ms, TE=440.8 ms, flip angle=58°, averages=2, time=30 min, echo chain length=120, matrix size=512×512×300, FOV=80 mm×80 mm, voxel size: 800 μm×800 μm×800 μm. At the same time, by comparing the histological sections with the MRI images, we found that the MRI images exhibited strong similarity with images from low magnification microscopy. With 3 T MRI images, this could be helpful for locating the boundaries of deep brain nuclei due to the large volume of brain tissue in non-human primates. However, in order to explore the spatial location of deep nuclei in the brain, high-resolution MRI is also necessary.

To discriminate the fine structures of the subcortical nuclei, the ROIs of the hippocampus, amygdala, and BLA were segmented and depicted (Figure 1C). The boundaries of the sROIs were manually delineated for each image in the horizontal plane. The volumes of the sROIs were then obtained in ITK-SNAP after completing segmentation. As the sample brains were formalin-fixed and firmly attached in the device during the MRI scans, there were no respiratory disturbances, as are found in live monkeys, so averaging the multiple scans significantly improved the SNR. Thus, the volumes of the hippocampus, amygdala, claustrum, and amygdala subfields were more precise using the 9.4 T MRI images due to the higher resolution and smaller error of the ultra-high magnetic field strength.

In this study, using ultra-high-resolution 9.4 T MRI, we

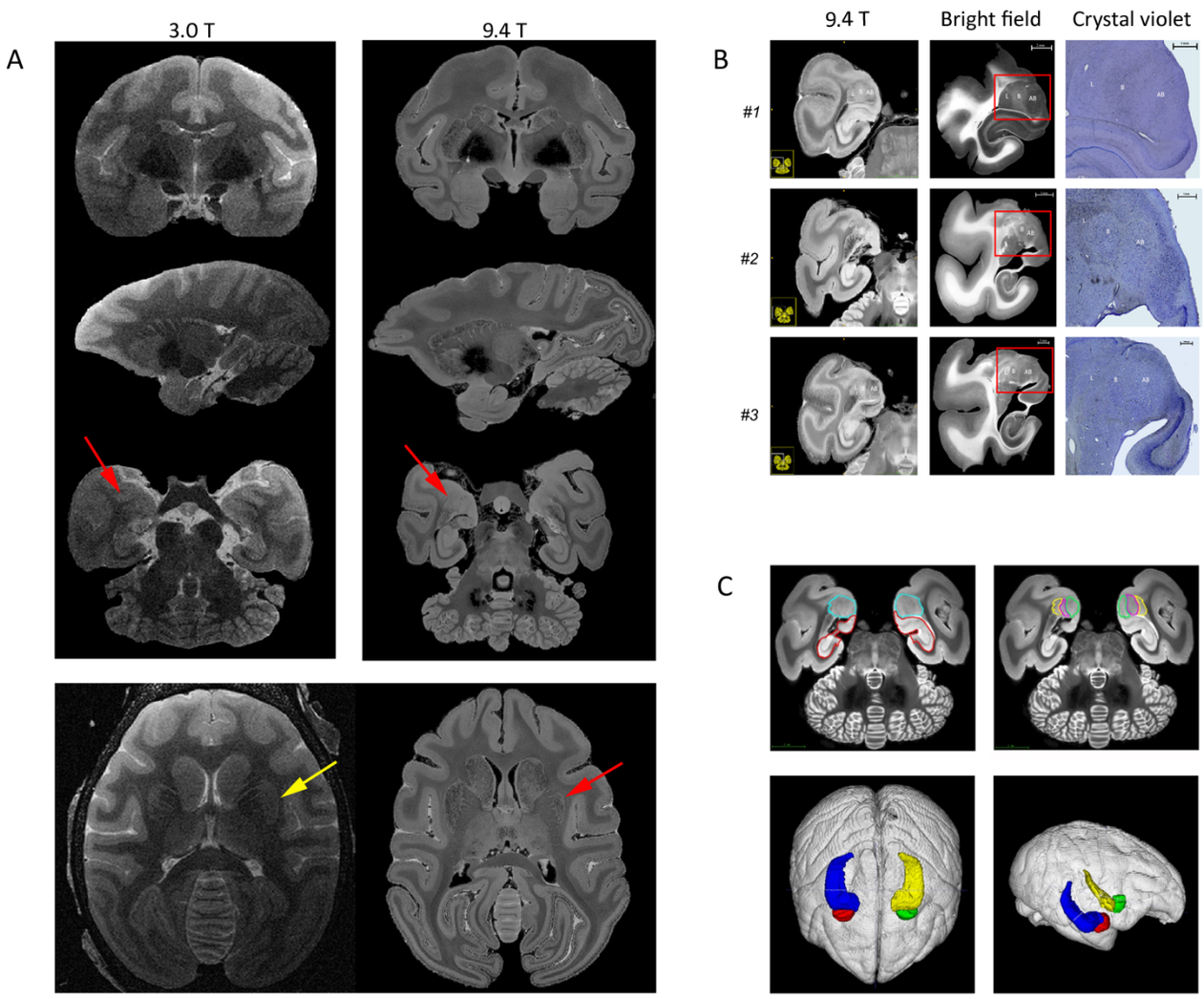

Figure 1 Comparison of 3 T and 9.4 T MRI images of rhesus monkey brains

A: MRI images of coronal (top row), sagittal (middle row), and horizontal (bottom row) planes acquired at 3 T 3D FLASH (left column) and 9.4 T 3D FLASH (right column). Red arrows indicate location of amygdala. Amygdala subfields are more easily identified on 9.4 T MRI images than on 3 T MRI images. Region (reconstruction voxel size: 310 μm×310 μm×300 μm, yellow arrow) of claustrum is obscured in 3 T MRI slice, especially right side of brain. In contrast, 9.4 T MRI images (voxel size: 155 μm×155 μm×155 μm, red arrow) easily show boundary of claustrum. B: Representative images of 9.4 T 2D FLASH MRI, bright field (black background), and crystal violet staining of right amygdala at each age stage. One monkey brain from each age group was selected for section staining. Each row represents right-side of amygdala of sample brain, which was cut and photographed. Left column shows horizontal MRI images close to position of sections in middle column. Middle column shows sections before staining. Staining of ROIs in red frame is shown in right column. Subnuclei in amygdala can be seen clearly on MRI images and sections before and after crystal violet staining (amygdala subfield: L: Lateral nuclei, B: Basal nuclei, AB: Accessory basal nuclei). Scale bars: 1 mm. C: Manual segmentation of amygdala and hippocampus. With high-resolution, 9.4 T MRI images show clear boundaries of each amygdala subregion. 3D models show exact positions of bilateral amygdala and hippocampus in monkey brains.

observed the fine structures in the amygdala, hippocampus, and BLA in the rhesus macaque brain. In contrast, the fine structures were not sufficiently clear for segmentation when using 3 T MRI. Clinically, psychological disturbances related to emotion and memory usually involve the amygdala, hippocampus, and their association (Sharp 2017; Yang & Wang, 2017). The BLA is the information entrance to the amygdala from the cortex and subcortical regions, such as the hippocampus. The lateral nucleus in the BLA is responsible for receiving extrinsic sensory information from the sensory thalamus and sensory cortices, and for output to other amygdala nuclei, including the basal and accessory basal nuclei (Janak & Tye, 2015; Pitkanen & Amaral, 1998). The BLA has reciprocal connections with the cortex and

hippocampus, and thus information from the BLA can have a broad influence throughout the cortex (Saunders et al., 1988). Thus, by segmentation of all deep nuclei within fine brain structures, we can accurately obtain their volumes.

The current study was based on high-resolution 9.4 T MRI scans of *ex-vivo* rhesus macaque brains. The next step will be to undertake anatomical research of rhesus macaque brains *in-vivo* and to obtain high-resolution MRI images over their entire lifespan. Such research can supplement histological studies, which can lose information on fine structural changes over long periods of time. In addition, because of the large volume of brain tissue in rhesus monkeys, tissue removal by optical techniques is not ideal for understanding the spatial structures of deep brain nuclei. Therefore, high-resolution MRI images are essential for studying the fine structures of the brain, especially deep nuclei.

In conclusion, our findings suggest that the use of ultra-high-resolution MRI images to display the microstructures of the brain is an essential technique. In the future, it would be interesting to identify the connections among subcortical nuclei in the brains of live macaques following behavioral training and testing using simultaneous fMRI.

COMPETING INTERESTS

The authors declare that they have no competing interests.

AUTHORS' CONTRIBUTIONS

J.L.L. and K.Z. initiated the project. H.Z.C. and H.Y.Y. designed the experiments. J.L.L. organized and supervised the whole project. H.Z.C. collected macaque brain samples and performed perfusion and fixation; H.Y.Y. and H.Z.C. performed MRI scanning and data collection; H.Z.C., K.Z., and J.L.L. drafted the manuscript, with input from all other authors. All authors read and approved the final version of the manuscript.

Huan-Zhi Chen[1,3], Hong-Yi Yang[2], Kai Zhong[2,5], Jia-Li Li[1,4,6,*]

[1] *Key Laboratory of Animal Models and Human Disease Mechanisms of Chinese Academy of Sciences* & *Yunnan Province*, *Kunming Institute of Zoology*, *Chinese Academy of Sciences*, *Kunming*, *Yunnan* 650223, *China*

[2] *High Magnetic Field Laboratory*, *Hefei Institutes of Physical Science*, *Chinese Academy of Sciences*, *Hefei*, *Anhui* 230031, *China*

[3] *Kunming College of Life Science*, *University of Chinese Academy of Sciences*, *Kunming*, *Yunnan* 650223, *China*

[4] *CAS Center for Excellence in Animal Evolution and Genetics*, *Chinese Academy of Sciences*, *Kunming*, *Yunnan* 650223, *China*

[5] *CAS Center for Excellence in Brain Science and Intelligence Technology*, *Chinese Academy of Sciences*, *Hefei*, *Anhui* 230031, *China*

[6] *Kunming Primate Research Center of the Chinese Academy of Sciences*, *Kunming Institute of Zoology*, *Chinese Academy of Sciences*, *Kunming*, *Yunnan* 650223, *China*

*Corresponding author, E-mail: lijiali@mail.kiz.ac.cn

REFERENCES

Huang Y, Coupland NJ, Lebel RM, Carter R, Seres P, Wilman AH, Malykhin NV. 2013. Structural changes in hippocampal subfields in major depressive disorder: a high-field magnetic resonance imaging study. *Biological Psychiatry*, **74**(1): 62−68.

Janak PH, Tye KM. 2015. From circuits to behaviour in the amygdala. *Nature*, **517**(7534): 284−292.

Knickmeyer RC, Styner M, Short SJ, Lubach GR, Kang C, Hamer R, Coe CL, Gilmore JH. 2010. Maturational trajectories of cortical brain development through the pubertal transition: unique species and sex differences in the monkey revealed through structural magnetic resonance imaging. *Cerebral Cortex*, **20**(5): 1053−1063.

Kwan BYM, Salehi F, Kope R, Lee DH, Sharma M, Hammond R, Burneo JG, Steven D, Peters T, Khan AR. 2017. Evaluation of ex-vivo 9.4 T MRI in post-surgical specimens from temporal lobe epilepsy patients. *Journal of Neuroradiology*, **44**(6): 377−380.

Pikkarainen M, Ronkko S, Savander V, Insausti R, Pitkanen A. 1999. Projections from the lateral, basal, and accessory basal nuclei of the amygdala to the hippocampal formation in rat. *The Journal of Comparative Neurology*, **403**(2): 229−260.

Pitkanen A, Amaral DG. 1998. Organization of the intrinsic connections of the monkey amygdaloid complex: projections originating in the lateral nucleus. *The Journal of Comparative Neurology*, **398**(3): 431−458.

Sah P, Faber ES, Lopez De Armentia M, Power J. 2003. The amygdaloid complex: anatomy and physiology. *Physiological Reviews*, **83**(3): 803−834.

Saleem KS, Logothetis NK. 2012. A Combined MRI and Histology Atlas of the Rhesus Monkey Brain in STereotaxic Coordinates. Amsterdam Boston: Academic Press.

Saunders RC, Rosene DL, Van Hoesen GW. 1988. Comparison of the efferents of the amygdala and the hippocampal formation in the rhesus monkey: II. Reciprocal and non-reciprocal connections. *The Journal of Comparative Neurology*, **271**(2): 185−207.

Sharp BM. 2017. Basolateral amygdala and stress-induced hyperexcitability affect motivated behaviors and addiction. *Translational Psychiatry*, **7**(8): e1194.

Shaw P, Kabani NJ, Lerch JP, Eckstrand K, Lenroot R, Gogtay N, Greenstein D, Clasen L, Evans A, Rapoport JL, Giedd JN, Wise SP. 2008. Neurodevelopmental trajectories of the human cerebral cortex. *The Journal of Neuroscience: The Official Journal of the Society for Neuroscience*, **28**(14): 3586−3594.

Sowell ER, Thompson PM, Peterson BS, Mattson SN, Welcome SE, Henkenius AL, Riley EP, Jernigan TL, Toga AW. 2002a. Mapping cortical gray matter asymmetry patterns in adolescents with heavy prenatal alcohol exposure. *NeuroImage*, **17**(4): 1807−1819.

Sowell ER, Thompson PM, Rex D, Kornsand D, Tessner KD, Jernigan TL, Toga AW. 2002b. Mapping sulcal pattern asymmetry and local cortical surface gray matter distribution in vivo: maturation in perisylvian cortices. *Cerebral Cortex*, **12**(1): 17−26.

Yang Y, Wang JZ. 2017. From structure to behavior in basolateral amygdala-hippocampus circuits. *Frontiers in Neural Circuits*, **11**: 86.